

Channel Customization for Joint Tx-RISs-Rx Design in Hybrid mmWave systems

Weicong Chen, Chao-Kai Wen, Xiao Li, and Shi Jin

Abstract—In strong line-of-sight millimeter-wave (mmWave) wireless systems, the rank-deficient channel severely hampers spatial multiplexing. To address this inherent deficiency, distributed reconfigurable intelligent surfaces (RISs) are introduced in this study to customize the wireless channel. Capitalizing on the ability of the RIS to reshape electromagnetic waves, we theoretically show that a favorable channel with an arbitrary tunable rank and a minimized truncated condition number can be established by elaborately designing the placement and reflection matrix of RISs. Different from existing works on distributed RISs, the number of elements needed for each RIS to combat the path loss and the limited phase control is also considered in this research. On the basis of the proposed channel customization, a joint transmitter-RISs-receiver (Tx-RISs-Rx) design under a hybrid mmWave system is investigated to maximize the downlink spectral efficiency. Using the proposed scheme, the optimal singular value decomposition-based hybrid beamforming at the Tx and Rx can be easily obtained without matrix decomposition for the digital and analog beamforming. The bottoms of the sub-channel mode in the water-filling power allocation algorithm, which are conventionally uncontrollable when the noise power is fixed, are proven to be independently adjustable by RISs. Moreover, the transmit power required for realizing multi-stream transmission is derived. Numerical results are presented to verify our theoretical analysis and exhibit substantial gains over systems without RISs.

Index Terms—Mmwave, rank deficiency, channel customization, reconfigurable intelligent surface, hybrid beamforming

I. INTRODUCTION

Since Shannon defined the maximum information transfer rate of a communication channel [1], the entire communication industry has been constantly improving and approaching the Shannon limit. According to Shannon's definition, the maximum information transfer rate, or channel capacity, depends on the signal-to-noise-ratio (SNR) and bandwidth of the channel. Thus, improving the SNR and increasing the bandwidth are two straightforward approaches to enlarge the capacity. However, logarithmic scaling indicates a rapidly diminishing gain obtained from SNR, and the commercial bandwidth is limited and expensive. Consequently, the multichannel triggered by the multiple-input-multiple-output (MIMO) technology was explored to pave a new way for capacity promotion [2]. In MIMO systems, the capacity grows linearly with the number of multichannels determined by the rank of the channel [3]. Nevertheless, when the troika (SNR, bandwidth, and multichannel) steps into millimeter-wave (mmWave) MIMO systems, new dilemmas emerge.

MmWave has been regarded as a promising advancement for future wireless communication systems. In contrast to the sub-6 GHz where the spectrum is extremely scarce, mmWave spectra above 20 GHz can provide multiple frequency bands with bandwidth up to 1–2 GHz, which offers extreme broadband capacity [4][5]. Although promising, the coverage of transmission in mmWave spectra shrinks due to severe path loss [6]. Equipping a large-scale antenna array [7]–[9] to provide more array gains is a key solution to improve the transmission rate and communication distance. Considering that the upper limit of the channel rank is imposed by the minimum number of antennas, the high SNR, broad bandwidth, and massive antennas in mmWave MIMO systems are supposed to enhance the capacity significantly. However, the channel rank is also constrained by the number of propagation paths. The combination of high gain beams and sparse channel in mmWave systems severely reduces the multichannel number, which may plummet to 1 in the strong line of sight (LoS) scenario regardless of the increasing antennas. The crux of spatial multiplexing provided by the multichannel lies in the channel that has been conventionally modeled as an uncontrollable exogenous entity that can only be adapt to. This iron law for the uncontrollable channel is broken by the burgeoning reconfigurable intelligent surface (RIS).

RIS, also known as passive large intelligent surface (LIS) [10] or intelligent reflecting surface (IRS) [11], has been envisaged to realize the so-called smart radio environment [12] that has become part of the system design parameters. It has been used to transform the channel for achieving multifarious tasks in various scenarios [13]–[23]. To enhance the coverage in mmWave systems, [13] and [14] introduced RIS to alleviate the significant path loss and severe blockage, respectively. In [15] and [16], RISs were used for beamforming and broadcasting, and the corresponding large-scale fading models were provided together with measurement verifications. In [17], RIS was utilized to create friendly multipaths for enhancing the secrecy rate of directional modulation. In multi-user scenarios, the maximization problem for the sum rate [18], the weight sum rate [19], the energy efficiency [20], the minimum signal-to-interference-plus-noise [21], the minimization problem for the average transmit power [22], and the maximum learning error [23] were investigated by optimizing the reflection matrix of the RIS.

Most of the aforementioned works mainly focused on solving optimization problems and merely illustrated how the RIS can reshape the channel. A joint transceiver and RIS design that can realize a favorable propagation environment with a small channel matrix condition number was reported in [24]. By deploying multiple RISs in the channel, [25]–[27] showed that the channel rank can be improved. Meanwhile, [28] examined the maximization of the effective rank and the minimum singular value of

Weicong Chen, Xiao Li, and Shi Jin are with the National Mobile Communications Research Laboratory, Southeast University, Nanjing 210096, China (e-mail: cwc@seu.edu.cn; li_xiao@seu.edu.cn; jinshi@seu.edu.cn).

Chao-Kai Wen is with the Institute of Communications Engineering, National Sun Yat-sen University, Kaohsiung City 80424, Taiwan (e-mail: chaokai.wen@mail.nsysu.edu.tw).

the RIS-augmented channel by using gradient-based optimization. With an RIS placed inside a random environment, the authors in [29] experimentally demonstrated that the disorder environments can be tuned to achieve optimal channel diversity by physically shaping the propagation medium itself. Unfortunately, no existing works have theoretically explained how the reflection phases of the RIS determine the characteristics of the channel, such as its condition number, rank, or effective rank.

Motivated by the intrinsic rank deficiency in the strong LoS mmWave channel and the potential of RISs in reshaping the channel, we study the channel customization to configure a favorable wireless propagation environment for a joint transmitter-RISs-receiver (Tx-RISs-Rx) design in the distributed RISs-assisted mmWave system. The contributions of this work are summarized as follows.

- A channel customization method is proposed to modify singular values of the composite channel between the Tx and Rx in three strong LoS mmWave scenarios with different antenna configurations. We demonstrate that by carefully designing the reflection matrix, set segmentation, and deployment location of the distributed RISs, the channel rank can be arbitrarily customized according to the number of data streams, and a well-conditioned channel with the minimum truncated condition number can be established.
- A joint Tx-RISs-Rx design scheme is developed under the hybrid mmWave architecture, which aims to maximize the downlink spectral efficiency (SE) by jointly devising the hybrid beamforming at the Tx and Rx, and the reflection phases of RISs. On the basis of the proposed channel customization, the optimal singular value decomposition (SVD) based hybrid beamforming can be easily separated into digital and analog beamforming without any matrix decomposition algorithms.
- The required transmit power for realizing s -stream transmission is derived. Different from the conventional water-filling power allocation, our channel customization method provides a novel way to change the bottom of the sub-channel mode individually by adjusting the tunable singular values. In such conditions, the transmit power threshold that enables the water level to cover s sub-channels modes is determined by s and the concrete design of the reflection matrix of RISs.
- Numerical results are presented to illustrate the effectiveness of the proposed channel customization and joint Tx-RISs-Rx design. With the help of RISs, a favorable channel with an arbitrary adjustable channel rank and a small truncated condition number can be customized. Furthermore, the joint Tx-RISs-Rx transmission scheme reaps substantial gains compared with conventional systems without RISs.

The rest of this paper is organized as follows. Section II introduces the system model. Then, the proposed channel customization and joint Tx-RISs-Rx design are presented in Sections III and IV, respectively. Afterward, Section V provides the numerical results for our proposal. Finally, Section VI concludes this study.

Notations: The vector and matrix are denoted by the lowercase and uppercase of a letter, respectively. $\text{tr}(\cdot)$ calculates the trace of a matrix. The transpose and conjugated-transpose operations are represented by superscripts $(\cdot)^T$ and $(\cdot)^H$, respectively. The superscripts $(\cdot)^A$ and $(\cdot)^D$ indicate parameters

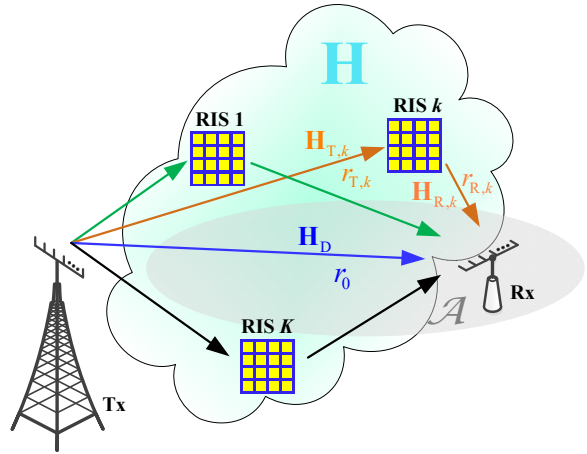


Fig. 1. Distributed RISs-assisted hybrid mmWave systems

that are associated with the angle-of-arrival (AoA) and angle-of-departure (AoD), respectively. $|\cdot|$ and $\|\cdot\|_F$ are used to indicate the absolute value and Euclidean norm, respectively. $\lceil \cdot \rceil$ is the integer ceiling. $\text{blkdiag}\{\mathbf{X}_1, \mathbf{X}_2, \dots, \mathbf{X}_N\}$ represents a block diagonal matrix with diagonal matrices \mathbf{X}_i , $i = 1, \dots, N$, while $\text{diag}(a_1, a_2, \dots, a_N)$ indicates a diagonal matrix with elements a_i , $i = 1, \dots, N$. The Kronecker product is denoted by \otimes .

II. SYSTEM MODEL

We consider a distributed RISs-assisted narrowband hybrid mmWave MIMO communication system, as shown in Fig. 1, where K RISs assist a multi-antenna Tx to serve a multi-antenna Rx. The Tx is equipped with N_T antennas and K_T radio frequency (RF) chains, and the Rx is equipped with N_R antennas and K_R RF chains, where $K_T < N_T$ and $K_R < N_R$. The uniform linear array (ULA) with element spacing being d_T and d_R is used at the Tx and Rx, respectively. Considering that the distances between Tx-RIS and RIS-Rx are different among RISs, we suggest that RISs be equipped with sufficient elements to combat the diverse path loss. Therefore, we assume that an $N_{S,k} (= N_{S,v,k} \times N_{S,h,k})$ -element uniform planar array (UPA) is equipped at RIS k , $k \in \mathcal{K} = \{1, 2, \dots, K\}$. The UPA for RIS k consists of $N_{S,v,k}$ rows and $N_{S,h,k}$ columns with all spacings being d_S . For system deployment, the Tx is settled at $\mathbf{e}_T = [x_T, y_T]^T$ in the Cartesian coordinates, the Rx's location $\mathbf{e}_R = [x_R, y_R]^T$ is randomly distributed in the coverage area \mathcal{A} , and the position of RIS k , $\mathbf{e}_{S,k} = [x_{S,k}, y_{S,k}]^T$, can be flexibly designed to customize the channel.

In the downlink, the received signal at the Rx is given by

$$\mathbf{y} = \mathbf{W}_{\text{BB}}^H \mathbf{W}_{\text{RF}}^H \mathbf{H} \mathbf{F}_{\text{RF}} \mathbf{F}_{\text{BB}} \mathbf{x} + \mathbf{W}_{\text{BB}}^H \mathbf{W}_{\text{RF}}^H \mathbf{n}, \quad (1)$$

where $\mathbf{x} = [x_1, x_2, \dots, x_s]^T \in \mathbb{C}^{s \times 1}$ satisfying $\mathbb{E}[\mathbf{x}\mathbf{x}^H] = \mathbf{I}$ is the transmitted signal from the Tx, $s \leq \min\{K_T, K_R\}$ is the number of data streams, and $\mathbf{F}_{\text{BB}} \in \mathbb{C}^{K_T \times s}$ ($\mathbf{W}_{\text{BB}} \in \mathbb{C}^{K_R \times s}$) and $\mathbf{F}_{\text{RF}} \in \mathbb{C}^{N_T \times K_T}$ ($\mathbf{W}_{\text{RF}} \in \mathbb{C}^{N_R \times K_R}$) are the digital and analog beamforming at the Tx (Rx), respectively. $\mathbf{H} \in \mathbb{C}^{N_R \times N_T}$ is the composite channel between the Tx and Rx, and $\mathbf{n} \in \mathbb{C}^{N_R \times 1} \sim \mathcal{CN}(0, \sigma^2 \mathbf{I})$ is the additive noise. The power constraint at the Tx is $\|\mathbf{F}_{\text{RF}} \mathbf{F}_{\text{BB}} \mathbf{x}\|_F^2 \leq E$, where E is the total transmit power.

A. Channel Model

In this study, we adopt the geometric model incorporating the Rician factor to describe the mmWave channel [30] [31]. As shown in Fig. 1, the composite channel \mathbf{H} contains the direct channel \mathbf{H}_D and the segmented reflection channels, $\mathbf{H}_{T,k}$ and $\mathbf{H}_{R,k}$. The Tx-RIS k channel can be expressed as

$$\mathbf{H}_{T,k} = \sqrt{N_T N_{S,k}} g_{T,k} \left(I_{T,k} \sqrt{\frac{\kappa_{T,k}}{\kappa_{T,k} + 1}} \mathbf{H}_{T,k}^{\text{LoS}} + \sqrt{\frac{1}{\kappa_{T,k} + 1}} \mathbf{H}_{T,k}^{\text{NLoS}} \right), \quad (2)$$

where $g_{T,k} = 1/\sqrt{4\pi r_{T,k}^2}$ [32] is the path loss¹ determined by distance $r_{T,k}$, whose unit is the wavenumber. The Rician factor $\kappa_{T,k}$ denotes the power ratio of the LoS component $\mathbf{H}_{T,k}^{\text{LoS}}$ and non-LoS (NLoS) component $\mathbf{H}_{T,k}^{\text{NLoS}}$. $I_{T,k} \in [0, 1]$ represents the probability of the existence of the LoS path. $\mathbf{H}_{T,k}^{\text{LoS}} = \mathbf{a}_{S,k}(\Phi_{T,k}^A, \Theta_{T,k}^A) \mathbf{a}_T^H(\Theta_{T,k}^D)$ and $\mathbf{H}_{T,k}^{\text{NLoS}} = \frac{1}{L_{T,k}} \sum_{l=1}^{L_{T,k}} \beta_{T,k,l} \mathbf{a}_{S,k}(\Phi_{T,k,l}^A, \Theta_{T,k,l}^A) \mathbf{a}_T^H(\Theta_{T,k,l}^D)$, where $\beta_{T,k,l} \in \mathcal{CN}(0, 1)$, $L_{T,k}$ is the number of NLoS paths. $\mathbf{a}_{S,k}(\cdot)$ and $\mathbf{a}_T(\cdot)$ are the array response vectors at RIS k and the Tx, respectively. In the array response vector, $\Phi_{T,k}^A = 2\pi d_S \cos \phi_{T,k}^A / \lambda$, $\Theta_{T,k}^A = 2\pi d_S \sin \phi_{T,k}^A \sin \theta_{T,k}^A / \lambda$, and $\Theta_{T,k}^D = 2\pi d_T \sin \theta_{T,k}^D / \lambda$, where $\phi_{T,k}^A$, $\theta_{T,k}^A$, and $\theta_{T,k}^D$ are the vertical AoA, horizontal AoA, and AoD in the LoS channel, respectively.

In analogy with the Tx-RIS k channel, the Rx-RIS k and Tx-Rx channels can be respectively given by

$$\mathbf{H}_{R,k} = \sqrt{N_R N_{S,k}} g_{R,k} \left(I_{R,k} \sqrt{\frac{\kappa_{R,k}}{\kappa_{R,k} + 1}} \mathbf{H}_{R,k}^{\text{LoS}} + \sqrt{\frac{1}{\kappa_{R,k} + 1}} \mathbf{H}_{R,k}^{\text{NLoS}} \right) \quad (3)$$

and

$$\mathbf{H}_D = \sqrt{N_T N_R} g_0 \left(I_D \sqrt{\frac{\kappa_D}{\kappa_D + 1}} \mathbf{H}_D^{\text{LoS}} + \sqrt{\frac{1}{\kappa_D + 1}} \mathbf{H}_D^{\text{NLoS}} \right), \quad (4)$$

where $\mathbf{H}_{R,k}^{\text{LoS}} = \mathbf{a}_R(\Theta_{R,k}^A) \mathbf{a}_{S,k}^H(\Phi_{R,k}^D, \Theta_{R,k}^D)$ and $\mathbf{H}_D^{\text{LoS}} = \mathbf{a}_R(\Theta_{R,0}^A) \mathbf{a}_T^H(\Theta_{T,0}^D)$ are LoS components, while $\mathbf{H}_{R,k}^{\text{NLoS}}$ and $\mathbf{H}_D^{\text{NLoS}}$ are NLoS components that have a similar expression to $\mathbf{H}_{T,k}^{\text{NLoS}}$. The array response for UPA can be decomposed into that of ULA as $\mathbf{a}_{S,k}(\Phi, \Theta) = \mathbf{a}_{S,v,k}(\Phi) \otimes \mathbf{a}_{S,h,k}(\Theta)$. The array response vector of ULA can be unified by

$$\mathbf{a}_X(Y) = \frac{1}{\sqrt{N_X}} \left[1, e^{jY}, \dots, e^{j(N_X-1)Y} \right]^T, \quad (5)$$

where $X \in \{\{T\}, \{R\}, \{S, v, k\}, \{S, h, k\}\}$.

As demonstrated in [34], individual channels $\mathbf{H}_{T,k}$, $\mathbf{H}_{R,k}$, and \mathbf{H}_D can be estimated accurately. Thus, after channel estimation, the composite channel consisting of K RISs can be expressed as

$$\mathbf{H} = \mathbf{H}_D + \sum_{k \in \mathcal{K}} \mathbf{H}_{R,k} \mathbf{\Gamma}_k \mathbf{H}_{T,k}, \quad (6)$$

¹This path loss model results in a cascaded path loss, which is proportional to the distances product from RIS k to the Tx and Rx, for the Tx-RIS k -Rx channel. This result is consistent with the model proposed in [16] and [33] for RISs.

where $\mathbf{\Gamma}_k \in \mathbb{C}^{N_{S,k} \times N_{S,k}}$ is the reflection matrix of RIS k . In practice, the continuous and element-level control of the reflection phase is costly to implement. For ease of practical implementation, we consider the column-control [35] with the reflection phase taken only from a finite number of discrete values. When column-level control is used, elements in the same column of the RIS are fed with the same control circuit. Thus, $\mathbf{\Gamma}_k = \mathbf{I} \otimes \text{diag}(e^{j\varpi_{k,1}}, \dots, e^{j\varpi_{k,N_{S,h,k}}})$, with $\varpi_{k,n}$ being the reflection phase of the n -th column. Assuming that the reflection phase is quantized by b bits, we obtain $\varpi_{k,n} \in \{2\pi i/2^b : i = 1, 2, \dots, 2^b\}$. In typical strong LoS mmWave communication systems, the LoS channel component always exists in the Tx-RIS, Rx-RIS, and Tx-Rx channels, that is, $I_{T,k} = I_{R,k} = I_D = 1$ holds for $\forall k \in \mathcal{K}$. Moreover, the Rician factor is sufficiently large, thus being able to ignore the NLoS component in such scenarios. For example, on the basis on the channel measurement in [36], the Rician factor can be set to 13.5 dB [14]. From these observations, we overlook the NLoS channel by setting $\kappa_{T,k}, \kappa_{R,k}, \kappa_D \rightarrow \infty$ in the following theoretical analysis to gain insights on channel customization and joint Tx-RISs-Rx design. The effects of NLoS will be evaluated in the numerical results.

In conventional mmWave communication systems without RISs, the rank of the channel between Tx and Rx will be reduced to 1 and cannot increase with the number of antennas when the strong LoS component dominates the channel. In these scenarios, the rank-deficient channel cannot provide spatial multiplexing to realize multi-stream transmission. Fortunately, the introduction of RISs produces a controllable scatters channel environment. By proactively designing the reflection matrices of RISs, a favorable communication environment can be established for multi-stream transmission. Given this consideration, we first investigate the design of RISs in the following sections to customize an arbitrary rank channel in strong LoS mmWave systems. After that, with a fixed number of data streams, we jointly design the transmit power at the Tx, the digital and analog beamforming at the Tx and Rx, as well as the reflection matrix at the RISs to maximize the downlink SE.

III. CHANNEL CUSTOMIZATION

For the spatial multiplexing promotion and the realization of multi-stream transmission in the strong LoS mmWave coverage, the composite channel should be devised so that the channel rank is no less than the data stream number. By applying the SVD, the composite channel can be represented by

$$\mathbf{H} = \hat{\mathbf{U}} \text{blkdiag} \{ \mathbf{\Lambda}, \mathbf{0}_{(N_T-Q) \times (N_R-Q)} \} \hat{\mathbf{V}}^H = \mathbf{U} \mathbf{\Lambda} \mathbf{V}^H, \quad (7)$$

where $\mathbf{\Lambda} = \text{diag}(\sqrt{\lambda_1}, \dots, \sqrt{\lambda_Q})$ is a $Q \times Q$ diagonal matrix with $\sqrt{\lambda_n}$ being the n -th largest non-zero singular value, \mathbf{U} and \mathbf{V} are formed by the first Q columns of the unitary matrices $\hat{\mathbf{U}} \in \mathbb{C}^{N_T \times N_T}$ and $\hat{\mathbf{V}} \in \mathbb{C}^{N_R \times N_R}$, respectively. According to the definition of rank, the number of non-zero singular values, Q , is the rank of \mathbf{H} . Consequently, even a tiny singular value can contribute one rank to the channel. In practical communication systems, the link quality of the sub-channel mode is proportional to its corresponding singular value. Thus, the sub-channel mode with a tiny singular value must not be used for transmitting data because of the poor channel condition. In other words, the channel rank cannot fully represent the maximal number of data streams.

To enhance the characterization of the composite channel \mathbf{H} , we adopt the effective rank [37], which is defined by

$$\text{Erank}(\mathbf{H}) = \exp\left(-\sum_n \bar{\lambda}_n \ln \bar{\lambda}_n\right), \quad (8)$$

where $\bar{\lambda}_n = \sqrt{\lambda_n} / \sum_m \sqrt{\lambda_m}$ is the singular value distribution of \mathbf{H} . With the effective rank, the contribution of a tiny singular value can be eliminated given that $\lim_{\bar{\lambda}_n \rightarrow 0} \bar{\lambda}_n \ln \bar{\lambda}_n = 0$. As proven in [37], the effective rank for a rank Q matrix will be maximal and equal to Q if and only if all non-zero singular values are equal. On the basis of the relation between rank and effective rank given an arbitrary number of data streams s , we define the truncated condition number as

$$T_s = \frac{\sqrt{\lambda_1}}{\sqrt{\lambda_s}}. \quad (9)$$

When $\lambda_i = \lambda_1$ for $\forall i \leq s$ and $\lambda_j = 0$ for $\forall j > s$, the truncated condition number achieves its minimum, that is, 1, and the effective rank is equal to the rank. In this case, the composite channel is favorable for the s -stream transmission. Therefore, we aim to minimize the truncated condition number by optimizing the deployment location and reflection matrices of RISs. To achieve this goal, the minimal number of elements for each RIS will also be derived for combating the path loss.

In the strong LoS mmWave MIMO systems where $I_{T,k} = I_{R,k} = I_D = 1$ and $\kappa_{T,k}, \kappa_{R,k}, \kappa_D \rightarrow \infty$, the composite channel in (6) can be simplified as

$$\begin{aligned} \mathbf{H} &= \sqrt{N_T N_R g_0} \mathbf{a}_R(\Theta_{R,0}^A) \mathbf{a}_T^H(\Theta_{T,0}^D) \\ &+ \sum_{k \in \mathcal{K}} \sqrt{N_R N_T N_{S,k} g_{R,k} g_{T,k}^*} \mathbf{a}_R(\Theta_{R,k}^A) \mathbf{a}_{S,k}^H(\Phi_{R,k}^D, \Theta_{R,k}^D) \\ &\times \mathbf{\Gamma}_k \mathbf{a}_{S,k}(\Phi_{T,k}^A, \Theta_{T,k}^A) \mathbf{a}_T^H(\Theta_{T,k}^D). \end{aligned} \quad (10)$$

Let $f(\mathbf{\Gamma}_k) \triangleq N_{S,k} \mathbf{a}_{S,k}^H(\Phi_{R,k}^D, \Theta_{R,k}^D) \mathbf{\Gamma}_k \mathbf{a}_{S,k}(\Phi_{T,k}^A, \Theta_{T,k}^A)$, $\alpha_0 \triangleq \sqrt{N_T N_R g_0}$, and $\alpha_k \triangleq \sqrt{N_T N_R g_{R,k} g_{T,k}^*} f(\mathbf{\Gamma}_k)$ being the array gain of RIS k , the path gain of the direct Tx–Rx channel, and the reconfigurable cascaded path gain of the Tx–RIS k –Rx channel, respectively, (10) can be unified as

$$\mathbf{H} = \sum_{k=0}^K \alpha_k \mathbf{a}_R(\Theta_{R,k}^A) \mathbf{a}_T^H(\Theta_{T,k}^D) = \mathbf{A}_R \mathbf{\Sigma} \mathbf{A}_T^H, \quad (11)$$

where $\mathbf{A}_R = [\mathbf{a}_R(\Theta_{R,0}^A), \mathbf{a}_R(\Theta_{R,1}^A), \dots, \mathbf{a}_R(\Theta_{R,K}^A)]$ is the array response matrix determined by the AoAs at the Rx, $\mathbf{A}_T = [e^{\angle \alpha_0} \mathbf{a}_T(\Theta_{T,0}^D), e^{\angle \alpha_1} \mathbf{a}_T(\Theta_{T,1}^D), \dots, e^{\angle \alpha_K} \mathbf{a}_T(\Theta_{T,K}^D)]$ is the phase-shifted array response matrix determined by the AoDs at the Tx, and $\mathbf{\Sigma} = \text{diag}(|\alpha_0|, |\alpha_1|, \dots, |\alpha_K|)$. The simplified composite channel in (11) is similar to the SVD in (7). When the columns of \mathbf{A}_R (\mathbf{A}_T) that correspond to the non-zero diagonal elements in $\mathbf{\Sigma}$ are pair-wisely orthogonal, $\mathbf{A}_R \mathbf{\Sigma} \mathbf{A}_T^H$ happens to be the SVD of \mathbf{H} , and the composite channel can be decoupled as several interference-free sub-channels. From this observation, we will investigate the orthogonality among columns in \mathbf{A}_R and in \mathbf{A}_T and customize the composite channel in terms of singular values for arbitrary multi-stream transmission. Given that the number of antennas affects the orthogonality of the array response vectors in \mathbf{A}_R and \mathbf{A}_T , we consider three scenarios with different

antenna configurations, that is, the extra-large scale MIMO (X-MIMO), the unilateral X-MIMO, and the conventional MIMO.

A. Channel Customization in the X-MIMO

The X-MIMO in this study refers to the scenario where the number of antennas at the Tx and Rx reaches infinity, while the number of RISs is limited, that is, $K \ll N_R, N_T \rightarrow \infty$.

For clarity of presentation, we first consider the general case where the Tx, RIS k , and Rx are not collinear. When the Tx and Rx are equipped with an extremely large number of antennas, we can easily prove that the array response vectors are asymptotically orthogonal [31], that is,

$$\begin{cases} \mathbf{a}_T^H(\Theta_{T,n}^D) \mathbf{a}_T(\Theta_{T,m}^D) \rightarrow 0, n \neq m \\ \mathbf{a}_R^H(\Theta_{R,i}^A) \mathbf{a}_R(\Theta_{R,j}^A) \rightarrow 0, i \neq j \end{cases}. \quad (12)$$

The asymptotical orthogonality of array response vectors at the Tx and Rx means that (11) is the SVD of \mathbf{H} . Hence, $\{|\alpha_k|\}_{k=0}^K$ are the singular values and $K+1$ is the maximal rank that can be achieved. Considering that α_0 is the constant path gain of the direct Tx–Rx channel that cannot be adjusted, the cascaded path gain of the Tx–RIS k –Rx channel should be carefully tuned to customize a favorable channel that has the maximum effective rank so that $|\alpha_k| = |\alpha_0|$ for $k \in \mathcal{K}$. Unfolding $|\alpha_k|$ and $|\alpha_0|$, the condition $|\alpha_k| = |\alpha_0|$ can be rewritten as

$$|f(\mathbf{\Gamma}_k)| = \frac{g_0}{g_{R,k} g_{T,k}} = \sqrt{4\pi} \frac{r_{R,k} r_{T,k}}{r_0}, \quad (13)$$

where the second equation is derived with the relation between path loss g and distance r . The absolute array gain of the RIS, $|f(\mathbf{\Gamma}_k)|$, is adjustable by the reflection matrix $\mathbf{\Gamma}_k$. Therefore, the prerequisite is that the maximum of $|f(\mathbf{\Gamma}_k)|$ should be no less than $\sqrt{4\pi} \frac{r_{R,k} r_{T,k}}{r_0}$ to make the condition (13) hold. Considering that RISs are column-controlled, without loss of generality, we assume that the Tx, RISs, and Rx are at the same height. The maximal achievable array gain of the RIS is provided in *Lemma 1*.

Lemma 1: When the Tx, RIS, and Rx are at the same height, for a sufficient large $N_{S,k}$ -elements RIS with column-level control and reflection phase quantized by b bits, the maximum of array gain is given by

$$f_{\max}(\mathbf{\Gamma}_k) = N_{S,k} \frac{2^b}{\pi} \sin \frac{\pi}{2^b} \quad (14)$$

Proof: When $\Phi_{R,k}^D = \Phi_{T,k}^A$, according to the definition of array gain of RIS k , we have

$$\begin{aligned} f(\mathbf{\Gamma}_k) &\triangleq N_{S,k} \mathbf{a}_{S,k}^H(\Phi_{R,k}^D, \Theta_{R,k}^D) \mathbf{\Gamma}_k \mathbf{a}_{S,k}(\Phi_{T,k}^A, \Theta_{T,k}^A) \\ &= N_{S,v,k} \sum_{n=1}^{N_{S,h,k}} e^{j(\varpi_{k,n} - (n-1)(\Theta_{R,k}^D - \Theta_{T,k}^A))}. \end{aligned} \quad (15)$$

It is easy to find that when the reflection phase of RISs can be continuously controlled,

$$\varpi_{k,n}^{\text{c,opt}} = (n-1)(\Theta_{R,k}^D - \Theta_{T,k}^A) \quad (16)$$

is the optimal reflection phase that turns $f(\mathbf{\Gamma}_k)$ to be the maximum, that is, $N_{S,k}$. However, when the resolution of the

reflection phase is constrained by b bits, the optimal discrete solution $\varpi_{k,n}^{\text{d,opt}}$ satisfies

$$-\frac{\pi}{2^b} \leq \varpi_{k,n}^{\text{d,opt}} - \varpi_{k,n}^{\text{c,opt}} \leq \frac{\pi}{2^b}. \quad (17)$$

When $N_{\text{S,h},k} \rightarrow \infty$, $\{\varpi_{k,n}^{\text{d,opt}} - \varpi_{k,n}^{\text{c,opt}}\}_{n=1}^{N_{\text{S,h},k}}$ will be uniformly distributed in $[-\frac{\pi}{2^b}, \frac{\pi}{2^b}]$. Thus, by setting the reflection phase as $\varpi_{k,n}^{\text{d,opt}}$ for $n \in \{1, \dots, N_{\text{S,h},k}\}$, we have

$$\begin{aligned} \lim_{N_{\text{S,h},k} \rightarrow \infty} \frac{f_{\max}(\mathbf{\Gamma}_k)}{N_{\text{S},k}} &= \lim_{N_{\text{S,h},k} \rightarrow \infty} \frac{1}{N_{\text{S,h},k}} \sum_{n=1}^{N_{\text{S,h},k}} e^{j(\varpi_{k,n}^{\text{d,opt}} - \varpi_{k,n}^{\text{c,opt}})} \\ &= \frac{2^b}{2\pi} \int_{-\frac{\pi}{2^b}}^{\frac{\pi}{2^b}} e^{jX} dX = \frac{2^b}{\pi} \sin \frac{\pi}{2^b}, \end{aligned} \quad (18)$$

which completes the proof. \blacksquare

Lemma 1 shows that the maximum of $|f(\mathbf{\Gamma}_k)|$ is determined by the scale of RISs, $N_{\text{S},k}$, and the quantization bits b . When $b \rightarrow \infty$, $f_{\max}(\mathbf{\Gamma}_k) \rightarrow N_{\text{S},k}$ can be derived for (14), which is consistent with the maximum array gain achieved with the continuously controlled reflection phase. Now, given the fixed quantization bits, we analyze the minimum scale of RISs that is required for (13) to combat the path loss and quantization loss. When the Tx and RISs are settled, $\{r_{\text{T},k}\}_{k=1}^K$ are constants while r_0 and $\{r_{\text{T},k}\}_{k=1}^K$ depend on the position of the Rx $\mathbf{e}_{\text{R}} \in \mathcal{A}$. To ensure that the favorable channel can be established for the Rx in every position of the coverage area, according to (13), the number of elements of RIS k should satisfy

$$N_{\text{S},k} \frac{2^b}{\pi} \sin \frac{\pi}{2^b} \geq \max_{\mathbf{e}_{\text{R}} \in \mathcal{A}} \left(\sqrt{4\pi} \frac{r_{\text{R},k} r_{\text{T},k}}{r_0} \right). \quad (19)$$

The right term of (19) varies in different scenarios because it depends on the geometric position and shape of the coverage area. To eliminate the tedious calculation for the rigorous lower bound constraint of $N_{\text{S},k}$ and obtain an easy system implementation, we set the number of elements of RIS k as

$$N_{\text{S},k} = \left\lceil \frac{\sqrt{4\pi^3}}{2^b \sin \frac{\pi}{2^b}} \frac{r_{\text{R},k}^{\max} r_{\text{T},k}}{r_0^{\min}} \right\rceil, \quad (20)$$

where $r_0^{\min} = \min_{\mathbf{e}_{\text{R}} \in \mathcal{A}}(r_0)$ and $r_{\text{R},k}^{\max} = \max_{\mathbf{e}_{\text{R}} \in \mathcal{A}}(r_{\text{R},k})$. Notably, $N_{\text{S},k}$ in (20) is a surplus guarantee for condition (19). When the reflection phase of the RIS is properly designed, such $N_{\text{S},k}$ enables Rx to achieve $|\alpha_k| = |\alpha_0|$ anywhere in the coverage because the array gain loss results from limited reflection phase quantization and the extra path loss brought by the distance product in the reflection link is compensated by more array gains provided by the increment of RIS elements.

On the basis of the RIS scale requirement (20), we now focus on the reflection phase design to customize a channel that has the maximal effective rank, which means that (13) should be satisfied for $k \in \mathcal{K}$. We split $f(\mathbf{\Gamma}_k)$ into two parts as

$$\begin{aligned} f(\mathbf{\Gamma}_k) &= N_{\text{S},\text{v},k} \sum_{n=1}^{\gamma_k} e^{j(\varpi_{k,n} - (n-1)(\Theta_{\text{R},k}^{\text{D}} - \Theta_{\text{T},k}^{\text{A}}))} \\ &\quad + N_{\text{S},\text{h},k} \sum_{n=\gamma_k+1}^{N_{\text{S},\text{h},k}} e^{j(\varpi_{k,n} - (n-1)(\Theta_{\text{R},k}^{\text{D}} - \Theta_{\text{T},k}^{\text{A}}))}, \end{aligned} \quad (21)$$

where $\gamma_k = \lceil \frac{\sqrt{4\pi^3}}{2^b \sin \frac{\pi}{2^b}} \frac{r_{\text{R},k} r_{\text{T},k}}{r_0 N_{\text{S},\text{v},k}} \rceil$. By designing the reflection phases of the first γ_k elements of RIS k as

$$\varpi_{k,n} = \varpi_{k,n}^{\text{d,opt}}, \quad (22)$$

the first term in the right of (21) can be approximated as $\sqrt{4\pi} \frac{r_{\text{R},k} r_{\text{T},k}}{r_0}$. To achieve (13), the second term in the right of (21) should be equal to 0. An infinite number of solutions exist for the design of the reflection phase of the last $N_{\text{S},\text{h},k} - \gamma_k$ RIS columns. Without loss of generality, $N_{\text{S},\text{h},k} - \gamma_k$ is assumed to be an even number, and one of the continuous solutions is

$$\varpi_{k,n} = (n - \gamma_k) \pi + \varpi_{k,n}^{\text{c,opt}}, \quad (23)$$

where $n \in \{\gamma_k + 1, \dots, N_{\text{S},\text{h},k}\}$. Under the limit of discrete reflection phases, we have

$$-\frac{\pi}{2^b} \leq \varpi_{k,n} - \left((n - \gamma_k) \pi + \varpi_{k,n}^{\text{c,opt}} \right) \leq \frac{\pi}{2^b}. \quad (24)$$

Similarly, when $N_{\text{S},\text{h},k}$ is sufficiently large and γ_k is limited, $\{\varpi_{k,n} - \varpi_{k,n}^{\text{c,opt}}\}_{\gamma_k+1}^{N_{\text{S},\text{h},k}}$ will be uniformly distributed in $[-\frac{\pi}{2^b}, \frac{\pi}{2^b}] \cup [\pi - \frac{\pi}{2^b}, \pi + \frac{\pi}{2^b}]$. In this case, we can prove that

$$\begin{aligned} \lim_{N_{\text{S},\text{h},k} \rightarrow \infty} \frac{1}{N_{\text{S},\text{h},k} - \gamma_k} \sum_{n=\gamma_k+1}^{N_{\text{S},\text{h},k}} e^{j(\varpi_{k,n} - \varpi_{k,n}^{\text{c,opt}})} \\ = \frac{2^b}{2\pi} \int_{-\frac{\pi}{2^b}}^{\frac{\pi}{2^b}} e^{jX} dX + \frac{2^b}{2\pi} \int_{\pi - \frac{\pi}{2^b}}^{\pi + \frac{\pi}{2^b}} e^{jX} dX = 0. \end{aligned} \quad (25)$$

Hence, the discrete design in (24) can sufficiently turn the second term of (21) to 0. At this point, the composite channel \mathbf{H} can be customized to have the maximum effective rank and equal singular values by utilizing (22) and (24) to design the reflection phases of the first γ_k and last $N_{\text{S},k} - \gamma_k$ columns of RIS k , respectively.

More than the aforementioned customization strategy, the composite channel can be flexibly shaped to let the effective rank be s when the Tx transmits s ($1 \leq s \leq K + 1$) data streams. Specifically, we divide the RISs into two sets, \mathcal{K}_{\perp} and $\bar{\mathcal{K}}_{\perp} = \mathcal{K} \setminus \mathcal{K}_{\perp}$, where $|\mathcal{K}_{\perp}| = s - 1$. For $i \in \mathcal{K}_{\perp}$, we design the reflection phases of RIS i according to (22) and (24) to let $|\alpha_i| = |\alpha_0|$. For $i \in \bar{\mathcal{K}}_{\perp}$, the reflection phases of RIS i is configured according to (24) so that $|\alpha_i| = 0$ can be guaranteed.

So far, channel customization has been discussed for non-collinear Tx, RIS k , and Rx. When the difference between the LoS AoDs of the Tx-Rx and Tx-RIS k channel is less than the array resolution of Tx, that is, $|\Theta_{\text{T},0}^{\text{D}} - \Theta_{\text{T},k}^{\text{D}}| \leq \frac{\pi}{N_{\text{T}}}$, the Tx, RIS k , and Rx are regarded as collinear. In this case, $\mathbf{a}_{\text{T}}(\Theta_{\text{T},0}^{\text{D}})$ and $\mathbf{a}_{\text{T}}(\Theta_{\text{T},k}^{\text{D}})$ are highly correlated, and the maximum rank of \mathbf{H} is reduced from $K + 1$ to K .

B. Channel Customization in the Unilateral X-MIMO

The unilateral X-MIMO refers to the scenario where the number of antennas at the Tx approaches infinity. The number of RISs is limited but larger than the number of antennas at the Rx, that is, $N_{\text{R}} < K \ll N_{\text{T}} \rightarrow \infty$. The maximal rank in the unilateral X-MIMO is N_{R} .

In the unilateral X-MIMO scenario, the asymptotical orthogonality is still tenable for array response vectors in \mathbf{A}_{T} but invalid for that in \mathbf{A}_{R} due to the limited number of antennas at the Rx.

Considering that $N_R < K$, the number of columns in \mathbf{A}_R is larger than its dimension, which means that the column vectors in \mathbf{A}_R must be linearly dependent. Thus, (11) is not the SVD of the composite channel.

Here, our target is to customize an effective rank s channel that can be explicitly expressed in the form of SVD by selecting $s-1$ RISs that generate good orthogonality among array response vectors in \mathbf{A}_R and reducing the array gains of the remaining RISs to avoid interference. Specifically, all RISs are divided into two sets, \mathcal{K}_\perp and $\bar{\mathcal{K}}_\perp$, which satisfy

$$\begin{cases} |\mathbf{a}_R^H(\Theta_{R,i}^A) \mathbf{a}_R(\Theta_{R,j}^A)| \approx 0, & i, j \in \mathcal{K}_\perp \cup \{0\}, i \neq j, \\ |\alpha_k| = 0, & k \in \bar{\mathcal{K}}_\perp, \end{cases} \quad (26)$$

where $|\mathcal{K}_\perp| = s-1$, $\mathcal{K}_\perp \cup \bar{\mathcal{K}}_\perp = \mathcal{K}$, and $\mathcal{K}_\perp \cap \bar{\mathcal{K}}_\perp = \emptyset$. On the basis of (26), the composite channel can be expressed in terms of SVD, that is,

$$\mathbf{H} = \sum_{k \in \mathcal{K}_\perp \cup \{0\}} \alpha_k \mathbf{a}_R(\Theta_{R,k}^A) \mathbf{a}_T^H(\Theta_{T,k}^D) = \mathbf{A}_{R,\perp} \boldsymbol{\Sigma}_\perp \mathbf{A}_{T,\perp}^H \quad (27)$$

where $\boldsymbol{\Sigma}_\perp$ is a diagonal matrix whose diagonal elements are $\{\alpha_k, k \in \mathcal{K}_\perp \cup \{0\}\}$. $\mathbf{A}_{R,\perp}$ and $\mathbf{A}_{T,\perp}$ are composed of orthogonal array response vectors that corresponded to $\{\alpha_k, k \in \mathcal{K}_\perp \cup \{0\}\}$. The key for channel customization (27) lies in the set division that satisfies (26). When the columns of a matrix \mathbf{A} are pair-wisely orthogonal, $\mathbf{A}^H \mathbf{A} = \mathbf{I}$. Therefore, to obtain $\mathbf{A}_{R,\perp}$ while avoiding $|\Theta_{T,0}^D - \Theta_{T,\bar{k}}^D| \leq \frac{\pi}{N_T}$, the RISs segmentation can be formulated as

$$\begin{aligned} \{\mathbf{A}_{R,\perp}, \mathcal{K}_\perp\} &= \arg \min_{\{\mathbf{A}, \mathcal{K}_{s-1}\}} \|\mathbf{A}^H \mathbf{A} - \mathbf{I}\|_F^2 \\ \text{s.t.} \quad \mathbf{A} &= [\mathbf{a}_R(\Theta_{R,0}^A), \mathbf{a}_R(\Theta_{R,k_1}^A), \dots, \mathbf{a}_R(\Theta_{R,k_{s-1}}^A)] \\ \mathcal{K}_{s-1} &= \{k_i\}_{i=1}^{s-1} \subseteq \mathcal{K} \setminus \{\bar{k}\} \end{aligned} \quad (28)$$

The optimal solution for the combinatorial optimization problem (28) requires exhaustive search over $\mathcal{K} \setminus \{\bar{k}\}$, which results in high search and computation complexity. To reduce this overhead, we resort to greedy search for (28). The greedy search algorithm is started by selecting RIS k_1 from $\mathcal{K} \setminus \{\bar{k}\}$ to ensure that $\mathbf{a}_R(\Theta_{R,k_1}^A)$ and $\mathbf{a}_R(\Theta_{R,0}^A)$ are approximately orthogonal, as discussed in (26). This process can be described by

$$\begin{aligned} \{\mathbf{A}_1, \mathcal{K}_1^*\} &= \arg \min_{\{\mathbf{A}, \mathcal{K}_1\}} \|\mathbf{A}^H \mathbf{A} - \mathbf{I}\|_F^2 \\ \text{s.t.} \quad \mathbf{A} &= [\mathbf{a}_R(\Theta_{R,0}^A), \mathbf{a}_R(\Theta_{R,k_1}^A)] \\ \mathcal{K}_1 &= \{k_1\} \subseteq \mathcal{K} \setminus \{\bar{k}\} \end{aligned} \quad (29)$$

After \mathbf{A}_1 and \mathcal{K}_1^* are found, another RIS denoted by k_2 can be obtained by executing (29) again with \mathbf{A} and \mathcal{K}_1 replaced by $[\mathbf{A}_1, \mathbf{a}_R(\Theta_{R,k_2}^A)]$ and $\mathcal{K}_1^* \cup \{k_2\}$, respectively. This greedy search process is performed until $s-1$ RISs, $\{k_i\}_{i=1}^{s-1}$, are selected. After that, we minimize the truncated condition number to customize the effective rank s channel by letting $|\alpha_i| = |\alpha_0|$ for $i \in \mathcal{K}_\perp$ and $|\alpha_i| = 0$ for $i \in \bar{\mathcal{K}}_\perp$. The procedure of the greedy search-based RISs segmentation is summarized in Algorithm 1.

The computational complexity of the exhaustive and greedy search is compared as follows. We consider the general case where the Tx, RISs, and the Rx are not collinear. Applying the

Algorithm 1 Greedy search-based RISs segmentation

Input: AoDs at the TX $\{\Theta_{T,k}^D\}_{k=0}^K$, AoAs at the Rx $\{\Theta_{R,k}^A\}_{k=0}^K$, the set of RISs \mathcal{K} , the required effective rank s , and the number of antennas at the Tx N_T .

Output: \mathcal{K}_\perp and $\bar{\mathcal{K}}_\perp = \mathcal{K} \setminus \mathcal{K}_\perp$.

1: Initial: $\mathcal{K}_\perp = \emptyset$, $\mathbf{A} = [\mathbf{a}_R(\Theta_{R,0}^A)]$, and $i = 1$;

2: Find RIS \bar{k} that are collinear with Tx and Rx, that is, $|\Theta_{T,0}^D - \Theta_{T,\bar{k}}^D| \leq \frac{\pi}{N_T}$

3: **while** $i \leq s-1$ **do**

4: $k_i = \arg \min_{k \in \mathcal{K} \setminus \{\bar{k}\}} \left\| [\mathbf{A}, \mathbf{a}_R(\Theta_{R,k}^A)]^H [\mathbf{A}, \mathbf{a}_R(\Theta_{R,k}^A)] - \mathbf{I} \right\|_F^2$;

5: $\mathcal{K}_\perp = \mathcal{K}_\perp \cup \{k_i\}$;

6: $\mathbf{A} = [\mathbf{A}, \mathbf{a}_R(\Theta_{R,k_i}^A)]$;

7: $i = i + 1$;

8: **end while**

exhaustive search scheme for (28), the search complexity is given by

$$\binom{K}{s-1} = \frac{K!}{(s-1)!(K-s+1)!} \quad (30)$$

In each search, computational complexity is dominated² by $\mathbf{A}^H \mathbf{A}$, that is, $\mathcal{O}(s^2 N_R)$. Therefore, the total computational complexity for the exhaustive search is

$$C_1 = \mathcal{O}\left(\frac{s^2 N_R K!}{(s-1)!(K-s+1)!}\right) \quad (31)$$

As a contrast, the search complexity of Algorithm 1 is $\sum_{i=1}^{s-1} (K-i+1)$. In the i -th search, the computational complexity is dominated by Line 4 in the Algorithm 1, which is $\mathcal{O}((i+1)^2 N_R)$. Consequently, the total computational complexity for the greedy search-based algorithm is

$$\begin{aligned} C_2 &= \mathcal{O}\left(\sum_{i=1}^{s-1} ((K-i+1)(i+1)^2 N_R)\right) \\ &= \mathcal{O}\left(N_R \left((K+1) \sum_{i=1}^{s-1} (i+1)^2 - \sum_{i=1}^{s-1} i(i+1)^2\right)\right) \end{aligned} \quad (32)$$

Utilizing $\sum_{k=1}^n k^2 = \frac{1}{6}n(n+1)(2n+1)$ and $\sum_{k=1}^n k(k+1)^2 = \frac{1}{12}n(n+1)(n+2)(3n+5)$ [38], (32) can be expressed as

$$\begin{aligned} C_2 &= \mathcal{O}\left(N_R \left((K+1) \frac{s(s+1)(2s+1)}{6} - 1 \right. \right. \\ &\quad \left. \left. - \frac{(s-1)s(s+1)(3s+2)}{12}\right)\right) \end{aligned} \quad (33)$$

Keeping the dominated component in (33), C_2 can be approximated by

$$C_2 = \mathcal{O}\left(\frac{N_R (4K-3s)s^3}{12}\right) \quad (34)$$

²The computational complexity for the Euclidean norm operation is $\mathcal{O}(s^3)$. Considering that s is much less than N_R in hybrid mmWave systems, this complexity can be neglected.

Comparing (34) with (31), we can see that adopting the greedy search-based algorithm can significantly reduce the computational complexity because the factorial operation is eliminated. To obtain an intuitive sense about the overhead reduction, by assuming $s = N_R = 8$ and $K = 25$, we have $C_1/C_2 \approx 9500$.

C. Channel Customization in the Conventional MIMO

The conventional MIMO refers to the scenario where the number of antennas at the Tx and Rx is limited. The number of RISs is larger than the number of antennas at the Rx but smaller than that at the Tx, that is, $N_R < K < N_T$.

In this case, the asymptotical orthogonality between array response vectors in \mathbf{A}_T and in \mathbf{A}_R is broken due to the limited number of antennas. We have shown in Section III-B that an approximate column-orthogonal matrix $\mathbf{A}_{R,\perp}$ can be generated through the RISs segmentation. Therefore, the only question left is how to ensure that array response vectors for the Tx-RIS channel are orthogonal.

We attempt to address this task via the system deployment of RISs. In the strong LoS mmWave communication systems, except for the direct link between the Tx-Rx channel, the columns of \mathbf{A}_T are determined by the positions of the Tx and RISs. On the basis of this observation, when the Tx is settled, we install RISs at the DFT directions of the Tx so that the AoD satisfies $\Theta_{T,k}^D \in \{\frac{2\pi i}{N_T} - \pi\}_{i=1}^{N_T}, k \in \mathcal{K}$. In this RISs deployment, we have

$$\mathbf{a}_T^H(\Theta_{T,k}^D) \mathbf{a}_T(\Theta_{T,m}^D) = 0 \quad (35)$$

for $k, m \in \mathcal{K}$ and $k \neq m$. Given the location of the Tx, $\mathbf{e}_T = [x_T, y_T]^T$, RIS k should be placed at $\mathbf{e}_{S,k} = [x_{S,k}, y_{S,k}]^T$, where

$$\begin{cases} x_{S,k} = r_{T,k} \cos\left(\arcsin \frac{\Theta_{T,k}^D}{\pi}\right) \\ y_{S,k} = r_{T,k} \frac{\Theta_{T,k}^D}{\pi} \end{cases} \quad (36)$$

So far, the composite channel in the conventional MIMO can be customized to have an effective rank s and the minimal truncated condition number by RISs deployment (equation (36)) and segmentation (Algorithm 1), as well as singular value modification ($|\alpha_i| = |\alpha_0|$ for $i \in \mathcal{K}_\perp$ and $|\alpha_k| = 0$ for $k \in \bar{\mathcal{K}}_\perp$).

IV. JOINT TX-RIS-RX DESIGN

Different from conventional communication systems, the introduction of RISs offers a new degree of freedom for designing transmission schemes in terms of reshaping channels. Given the potential of the flexible channel customization discussed in Section III, this subsection aims to maximize the downlink SE of s data streams by jointly designing the hybrid beamforming at the Tx and Rx and the reflection phases of RISs. The required transmit power for guaranteeing s -stream transmission is derived as well.

The conventional MIMO is considered, that is, $N_R < K < N_T$. Supposing that the transmitted s -stream signal follows a Gaussian distribution, the downlink SE is then given by

$$R = \log_2 \det(\mathbf{I} + \frac{1}{\sigma^2} \mathbf{W}_{BB}^H \mathbf{W}_{RF}^H \mathbf{H} \mathbf{F}_{RF} \mathbf{F}_{BB}) \times \mathbf{F}_{BB}^H \mathbf{F}_{RF}^H \mathbf{H}^H \mathbf{W}_{RF} \mathbf{W}_{BB}) \quad (37)$$

The SE maximization problem can be formulated as

$$\begin{aligned} & \max_{\mathbf{W}_{RF}, \mathbf{W}_{BB}, \{\Gamma_k\}_{k=1}^K, \mathbf{F}_{RF}, \mathbf{F}_{BB}} R \\ \text{s.t.} & \quad \|\mathbf{F}_{RF} \mathbf{F}_{BB}\|_F^2 \leq E, \\ & \quad \sqrt{N_T} |\mathbf{F}_{RF}(n, m)| = 1, \forall n, m, \\ & \quad \sqrt{N_R} |\mathbf{W}_{RF}(n, m)| = 1, \forall n, m, \\ & \quad \Gamma_k = \mathbf{I} \otimes \text{diag}\left(e^{j\varpi_{k,1}}, \dots, e^{j\varpi_{k,N_{S,h,k}}}\right). \end{aligned} \quad (38)$$

Such an optimization problem poses challenges in obtaining the optimal solution because the objective function R coupled with $K + 4$ matrix variables and the constant modulus constraints on \mathbf{F}_{RF} , \mathbf{W}_{RF} , and Γ_k are non-convex. Given the reflection phases of RISs $\{\Gamma_k\}_{k=1}^K$, the composite channel \mathbf{H} is fixed, and the optimal hybrid beamforming at the Tx and Rx can be obtained via the SVD of \mathbf{H} in (7). When $\{\Gamma_k\}_{k=1}^K$ are given and $Q \geq s$, the optimal hybrid beamforming at the Tx and Rx can be expressed as

$$\begin{aligned} \mathbf{F}_{RF} \mathbf{F}_{BB} &= \mathbf{V}_s \mathbf{P}^{1/2}, \\ \mathbf{W}_{RF} \mathbf{W}_{BB} &= \mathbf{U}_s, \end{aligned} \quad (39)$$

where \mathbf{V}_s and \mathbf{U}_s are the first s columns of \mathbf{V} and \mathbf{U} , respectively; $\mathbf{P} = \text{diag}(p_1, \dots, p_s)$ is the water-filling power allocation matrix. The diagonal element in \mathbf{P} is given by

$$p_i = \max\left(\mu - \frac{\sigma^2}{\lambda_i}, 0\right), \quad (40)$$

where μ is the water level that satisfies $\sum_{i=1}^s p_i = E$.

Although the optimal hybrid beamforming at the Tx and Rx can be designed via the SVD of \mathbf{H} , this design faces three challenges.

- The requirement for channel rank: To realize s -stream signal transmission, the channel rank should be larger than s , which is unattainable in the conventional strong LoS mmWave communication systems. As a result of the introduction of RISs, the channel rank can be customized, and the challenge thus lies in how to configure the reflection phases of RISs.
- The requirement for the minimum transmit power: The water-filling power allocation matrix depends on not only the singular values $\{\lambda_i\}_{i=1}^s$ but also the transmit power E . When the noise power is fixed while E continues to decrease, the water level μ continues falling so that only one data stream can be allocated with power even if the channel rank is larger than s . Therefore, the minimum transmit power should be derived to avoid zero power allocated to data streams.
- The decomposition of digital and analog beamforming: Although the hybrid beamforming at the Tx and Rx can be easily obtained as (39), it should be further decoupled into the digital and analog beamforming in the hybrid architecture. The matrix decomposition will inevitably lose the accuracy of the reconstructed hybrid beamforming and bring high computational complexity.

Aiming at these challenges, we attempt to satisfy the requirement for the channel rank by channel customization and derive a closed-form expression for the required transmit power. On the basis of channel customization, a low-complexity design for the digital and analog beamforming is proposed without matrix decomposition.

A. Joint Tx-RISs-Rx Design in the High SNR Regime

In the high SNR regime, the equal power allocation is asymptotically optimal, that is, $p_i = E/s$ [3]. In this case, substituting the SVD-based hybrid beamforming (39) into the SE (37), we have

$$R = \log_2 \det \left(\mathbf{I} + \frac{E}{s\sigma^2} \text{diag}(\lambda_1, \dots, \lambda_s) \right). \quad (41)$$

Utilizing $\log_2 \det(\text{diag}(x_1, \dots, x_s)) = \sum_{i=1}^s \log_2 x_i$ for (41), the original optimization problem in (38) can be expressed as

$$\begin{aligned} \max_{\{\Gamma_k\}_{k=1}^K} & \sum_{i=1}^s \log_2 \left(1 + \frac{E}{s\sigma^2} \lambda_i \right) \\ \text{s.t.} & \quad \Gamma_k = \mathbf{I} \otimes \text{diag} \left(e^{j\varpi_{k,1}}, \dots, e^{j\varpi_{k,N_{S,h,k}}} \right). \end{aligned} \quad (42)$$

In the conventional strong LoS mmWave communication system where the channel between the Tx and Rx is immutable, the objective function in (42) is a constant with $\lambda_1 \neq 0$ and $\lambda_i = 0$ for $i = 2, \dots, \min(N_T, N_R)$, which means only one data stream can be transmitted. With the help of RISs, singular values of the composite channel can be modified to establish a favorable channel for the multi-stream. However, in general cases, calculating the singular values, which is required in (42), does not have a closed-form expression with $\{\Gamma_k\}_{k=1}^K$ and must be calculated numerically, e.g., through an iterative algorithm, as specified in [39] and [40]. Furthermore, the channel rank should be larger than s . Having a closed-form expression of singular values is important for the SE maximization problem. To address this challenge, we use the proposed channel customization, which provides a good approximation of singular values.

To provide multi-stream transmission for the Rx in a specific coverage area, we follow the channel customization scheme proposed in Section III to deploy K RISs in the DFT directions of the Tx and apply the RISs segmentation algorithm to generate RISs sets \mathcal{K}_\perp and $\bar{\mathcal{K}}_\perp$. By configuring $|\alpha_i| = 0$ for $i \in \bar{\mathcal{K}}_\perp$, $\{\lambda_i\}_{i=1}^s$ can be approximated by $\{|\alpha_k|, k \in \mathcal{K}_\perp \cup \{0\}\}$, and $\mathbf{H} = \mathbf{A}_{R,\perp} \Sigma_\perp \mathbf{A}_{T,\perp}^H$ in (11) can be regarded as the SVD. On the basis of this customized composite channel, the optimal hybrid beamforming at the Tx and Rx can be easily designed without matrix decomposition, that is,

$$\begin{aligned} \mathbf{F}_{\text{BB}} &= \sqrt{\frac{E}{s}} \mathbf{I}, \mathbf{F}_{\text{RF}} = \mathbf{A}_{T,\perp}, \\ \mathbf{W}_{\text{BB}} &= \mathbf{I}, \mathbf{W}_{\text{RF}} = \mathbf{A}_{R,\perp}. \end{aligned} \quad (43)$$

Then, (42) can be rewritten as

$$\begin{aligned} \max_{\{\Gamma_k, k \in \mathcal{K}_\perp\}} & \sum_{i \in \mathcal{K}_\perp \cup \{0\}} \log_2 \left(1 + \frac{E}{s\sigma^2} |\alpha_i| \right) \\ \text{s.t.} & \quad \Gamma_k = \mathbf{I} \otimes \text{diag} \left(e^{j\varpi_{k,1}}, \dots, e^{j\varpi_{k,N_{S,h,k}}} \right). \end{aligned} \quad (44)$$

Considering that $|\alpha_k|$ is only determined by Γ_k , (44) can be decoupled into $s-1$ independent sub-problems. For RIS $k \in \mathcal{K}$, the sub-problem is given by

$$\begin{aligned} \max_{\Gamma_k} & \log_2 \left(1 + \frac{E}{s\sigma^2} |\alpha_k| \right) \\ \text{s.t.} & \quad \Gamma_k = \mathbf{I} \otimes \text{diag} \left(e^{j\varpi_{k,1}}, \dots, e^{j\varpi_{k,N_{S,h,k}}} \right). \end{aligned} \quad (45)$$

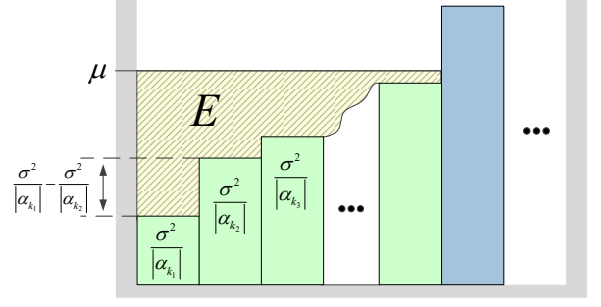


Fig. 2. Schematic diagram of water-filling power allocation algorithm.

The optimal solution for (45) is to maximize $|\alpha_k|$. Thus, the reflection phases of RIS k should be designed according to (17). Note that we do not claim the optimality of our joint Tx-RISs-Rx design because the reflection matrix of RISs for channel customization may not be the optimal solution in terms of SE. However, it has the advantages of completely removing the matrix decomposition complexity of the SVD-based hybrid beamforming at the Tx and Rx. More importantly, it allows for intuitive sensing of how RISs can change singular values of the composite channel. The closed-form expression for singular values can also be used to determine a reasonable transmit power for the s -stream transmission, as shown in the next subsection.

B. Required Transmit Power for Realizing the s -stream Transmission

In general cases, the SNR may be insufficient in guaranteeing the asymptotical optimality of equal power allocation. Following the channel customization and the SVD-based hybrid beamforming in Section IV-A and replacing the equal power allocation with the optimal water-filling algorithm, (44) should be modified as

$$\begin{aligned} \max_{\{\Gamma_k, k \in \mathcal{K}_\perp\}, \mathbf{P}} & \sum_{i \in \mathcal{K}_\perp \cup \{0\}} \log_2 \left(1 + \frac{|\alpha_i|}{\sigma^2} p_i \right) \\ \text{s.t.} & \quad p_i = \max \left(\mu - \frac{\sigma^2}{|\alpha_i|}, 0 \right), \\ & \quad \sum_{i \in \mathcal{K}_\perp \cup \{0\}} p_i = E, \\ & \quad \Gamma_k = \mathbf{I} \otimes \text{diag} \left(e^{j\varpi_{k,1}}, \dots, e^{j\varpi_{k,N_{S,h,k}}} \right). \end{aligned} \quad (46)$$

Fig. 2 illustrates the procedure of the water-filling power allocation algorithm, which pours the “water” E into the tank. The height from the bottom of the tank, $\sigma^2/|\alpha_{k_i}|$, to the water level μ is the power allocated to sub-channel mode k_i . When E continues to decrease, the bottom of the sub-channel modes will gradually break through the water lever μ , thus resulting in a decreasing number of available sub-channel modes. If the first altitude intercept is larger than the total number of “water,” that is, $(\sigma^2/|\alpha_{k_1}| - \sigma^2/|\alpha_{k_2}|) \geq E$, the total transmit power is allocated to only one data stream. Therefore, to realize the s -

stream transmission, E should be larger than a certain threshold E_{Th} so that the minimal power is larger than 0, that is,

$$p_{\min} = \mu - \frac{\sigma^2}{|\alpha_{\min}|} > 0, \quad (47)$$

where $|\alpha_{\min}|$ is the minimum of $|\alpha_i|$ for $i \in \mathcal{K}_{\perp} \cup \{0\}$. Considering that $N_{S,i}$ given in (20) enables $|\alpha_i| \geq |\alpha_0|$, $|\alpha_{\min}| = |\alpha_0|$ is assumed. In this case, according to the power constraint $\sum_i p_i$, the water level can be obtained as

$$\mu = \frac{E}{s} + \sum_{i \in \mathcal{K}_{\perp} \cup \{0\}} \frac{\sigma^2}{s|\alpha_i|}. \quad (48)$$

Substituting (48) into (47), we have

$$E > \frac{(s-1)\sigma^2}{|\alpha_0|} - \sum_{i \in \mathcal{K}_{\perp}} \frac{\sigma^2}{|\alpha_i|} = E_{\text{Th}} \quad (49)$$

Except for s , the threshold E_{Th} is also determined by path gains $\{|\alpha_i|, i \in \mathcal{K}_{\perp} \cup \{0\}\}$. As a result, E_{Th} will vary with the reflection matrices $\{\Gamma_i, i \in \mathcal{K}_{\perp}\}$. Nevertheless, when E is larger than the maximum of E_{Th} , $p_i > 0$ will always hold for $i \in \mathcal{K}_{\perp} \cup \{0\}$ given any Γ_i constrained by $|\alpha_i| \geq |\alpha_0|$. The maximized $|\alpha_i|$ turns E_{Th} into the maximum. Thus, the maximal E_{Th} can be obtained as

$$\begin{aligned} E_{\text{Th}}^{\max} &= \frac{(s-1)\sigma^2}{|\alpha_0|} - \sum_{i \in \mathcal{K}_{\perp}} \frac{\sigma^2}{|\alpha_{i,\max}|} \\ &= \frac{\sigma^2}{\sqrt{N_{\text{T}}N_{\text{R}}}} \left(\frac{s-1}{g_0} - \sum_{i \in \mathcal{K}_{\perp}} \frac{1}{N_{S,i}g_{R,i}g_{T,i} \frac{2^b}{\pi} \sin \frac{\pi}{2^b}} \right) \\ &= \sqrt{\frac{4\pi}{N_{\text{T}}N_{\text{R}}}} \sigma^2 \left(r_0(s-1) - \sum_{i \in \mathcal{K}_{\perp}} \frac{r_{R,i}r_{T,i}\sqrt{4\pi^3}}{N_{S,i}2^b \sin \frac{\pi}{2^b}} \right), \end{aligned} \quad (50)$$

where $|\alpha_{i,\max}|$ is the maximum of $|\alpha_i|$ by setting $|f(\Gamma_i)|$ as the maximum according to (17). When system parameters are fixed, we can see that E_{Th}^{\max} is determined by the distances from the Rx to the Tx and to RISs. In other words, different positions in the coverage require different levels of the transmit power for the Rx to realize the s -stream transmission. Fig. 3 explains why E_{Th}^{\max} enables $p_i > 0$ for $i \in \mathcal{K}_{\perp} \cup \{0\}$ given any Γ_i constrained by $|\alpha_i| \geq |\alpha_0|$. When $E = E_{\text{Th}}^{\max}$ and $\Gamma_i, i \in \mathcal{K}_{\perp}$, is configured to achieve $|\alpha_i| = |\alpha_{i,\max}|$, the water level will reach exactly the bottom of the sub-channel mode that corresponds to the direct link between the Tx and Rx. In this case, arbitrary modifications on the Γ_i will lead to $|\alpha_i| < |\alpha_{i,\max}|$, thus raising the bottom of its corresponding sub-channel mode. Once the bottom of the effective sub-channel mode rises, the water level must be elevated to overwhelm the bottom $\sigma^2/|\alpha_0|$, which means $p_i > 0$ holds for $i \in \mathcal{K}_{\perp} \cup \{0\}$.

In the following, $c \in \bar{\mathcal{K}}_{\perp}$ is assumed to not break the orthogonality of $\mathbf{A}_{R,\perp}$ when it is enrolled into \mathcal{K}_{\perp} . Then, when another data stream is demanded, we can set $|\alpha_c| = |\alpha_{c,\max}|$ to generate an additional sub-channel mode with the bottom being $\sigma^2/|\alpha_{c,\max}|$. In this case, the difference between the maximal

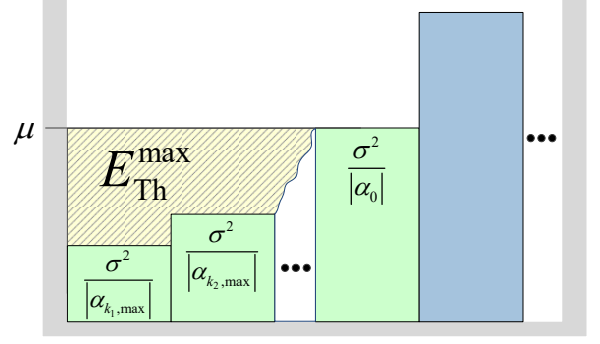


Fig. 3. A critical point for water-filling power allocation algorithm.

thresholds for $s+1$ and s data streams satisfies

$$\begin{aligned} \Delta E_{\text{Th}}^{\max} &= E_{\text{Th}}^{\max}|_{s+1} - E_{\text{Th}}^{\max}|_s \\ &= \sqrt{\frac{4\pi}{N_{\text{T}}N_{\text{R}}}} \sigma^2 \left(r_0 - \frac{r_{R,c}r_{T,c}\sqrt{4\pi^3}}{N_{S,c}2^b \sin \frac{\pi}{2^b}} \right). \end{aligned} \quad (51)$$

This extra transmit power required for another data stream depends on the chosen RIS c and the position of the Rx because they determine $N_{S,c}$, $r_{R,c}$, and r_0 . When the scale of RIS c , $N_{S,c}$, is increased, the demand for extra transmit power increased. In the extreme case where $N_{S,c} \rightarrow \infty$, we have $\Delta E_{\text{Th}}^{\max} \rightarrow \sigma^2/|\alpha_0|^2$. Fig. 3 can explain this phenomenon as well. Digging up another sub-channel mode that has a bottom $\sigma^2/|\alpha_{c,\max}|$ below the original water level will inevitably bring down the water level and expose the bottom of the highest sub-channel mode to the air. To overwhelm the exposed sub-channel mode again, the water should increase accordingly. Considering that increasing $N_{S,c}$ will depress the bottom $\sigma^2/|\alpha_{c,\max}|$, this water increment will increase with $N_{S,c}$ and reach its limited imposed by $\sigma^2/|\alpha_0|^2$.

In the above scenario, another data stream is obtained at the cost of the transmit power increment in the condition that $|\alpha_i| = |\alpha_{i,\max}|$ for $i \in \mathcal{K}_{\perp}$. This result is common in a traditional water-filling algorithm. However, with the channel customization ability of RISs, we can transmit additional data streams without enlarging the transmit power for the water-filling algorithm. Different from the conventional system where the bottom of the sub-channel is uncontrollable, RISs can individually elevate the bottoms so that when another sub-channel is dug out, the water level can be pushed back to the original position without pouring additional water into the tank. From this point of view, customizing a composite channel with homogenous singular values, or a minimized truncated condition number, is the ideal condition for guaranteeing the multi-stream transmission. However, this strategy fails to achieve the maximum singular value for some sub-channels, thus inevitably resulting in a deteriorative SE, as will be illustrated in Section V.

V. NUMERICAL RESULTS

In this section, numerical results are presented to demonstrate the effectiveness of the proposed channel customization and joint Tx-RISs-Rx design in the rank deficient strong LoS mmWave communication system. The conventional MIMO is considered,

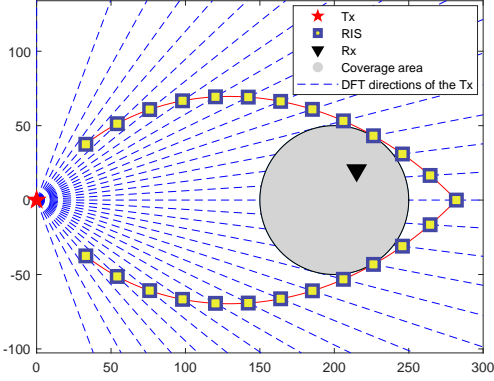


Fig. 4. System deployment (top view).

that is, $N_R < K < N_T$. The system carrier frequency is $f_c = 28$ GHz. As shown in Fig. 4, the Tx, equipped with $N_T = 32$ antennas and $K_T = 8$ RF chains, is located in the original Cartesian coordinates $\mathbf{e}_T = [0, 0]^T$. DFT directions of the Tx are represented by a series of rays emitted from \mathbf{e}_T with the angle being $\xi \in \{\arcsin(\frac{2i}{N_T} - 1), i = 1, \dots, N_T\}$. The Rx is assumed to be randomly distributed in a circular coverage with the center and the radius being $\mathbf{e}_C = [200, 0]^T$ and $r_C = 50$, respectively. The Rx is equipped with $N_R = 8$ antennas and $K_R = s$ RF chains. Twenty-five RISs are mounted in the system. To deploy these RISs, a curve \mathcal{S} that has 25 intersections with the DFT directions is provided in Fig. 4 as an example. The coordinates of \mathcal{S} are given by $\mathbf{e}_S = [\rho \cos \varepsilon, \rho \sin \varepsilon]^T$ for $\varepsilon \in [-\varepsilon_{\max}, \varepsilon_{\max}]$, where $\varepsilon_{\max} = \arcsin((K + 1)/N_T)$ is the angle of the first intersection and $\rho = 50 + (282 - 50)(1 - |\varepsilon|/\varepsilon_{\max})$ is the distance from \mathbf{e}_S to the Tx. According to Section III-C, we place 25 RISs at these intersections, respectively. Given the fixed positions of the Tx and RISs, and the range of coverage, the number of elements required for RISs to combat the path loss is given by (20). The AoA and AoD of the LoS paths are determined by the locations of the Tx, Rx, and RISs while those of the NLoS paths are randomly distributed in $\mathcal{U}[0, \pi]$. The elements' distance for all ULAs is set as half wavelength. The noise power is normalized as $\sigma^2 = 1$.

Considering that the channel customization is purpose-oriented, in the following, we focus on two scenarios where the reflection phases of RISs in \mathcal{K}_\perp ($|\mathcal{K}_\perp| = s - 1$) are designed to achieve homogeneous path gains (HPG) to minimize the truncated condition number T_s or maximal path gains (MPG) to maximize the SE R . More specifically, HPG and MPG indicate $\{|\alpha_i| = |\alpha_0|, |\alpha_j| = 0\}$ and $\{|\alpha_i| = |\alpha_{i,\max}|, |\alpha_j| = 0\}$, respectively, for $i \in \mathcal{K}_\perp$, $j \in \mathcal{K} \setminus \mathcal{K}_\perp$. The randomly designed reflection phases that result in random path gains (RPG) are considered the worst case when the SE is assessed.

A. Channel Customization

In this subsection, we evaluate the channel customization in terms of the effective rank and the truncated condition number. Assuming that the number of data streams s increases from 2 to 8, we plot in Fig. 5 the CDF of the rank and effective rank of the composite channel that has been customized according to s .

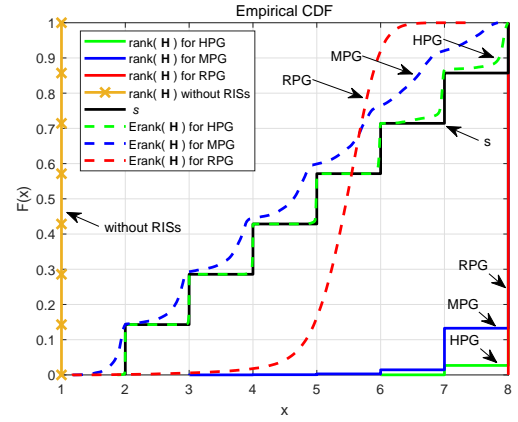


Fig. 5. CDF of the rank and effective rank of the composite channel that has been customized according to s .

For each s , the Monte Carlo simulation is performed for 10,000 channel realizations by randomly placing the Rx in the coverage. The solid lines except for the stair curve for s are the CDF of the channel rank, which is the number of non-zero singular values, and calculated by MATLAB. Meanwhile, the dashed lines are the CDF of the effective rank determined by (8).

From Fig. 5, we see that the rank for RPG has always been 8, thus indicating a full column rank for the composite channel. However, this full column rank is deceptive because the effective rank for RPG is mainly distributed between 5 and 6. In 70,000 channel realizations, by randomly designing the reflection phases, over 80% of channels have an effective rank that is larger than 5, thus showing an excellent channel improvement at first sight because the channel rank is 1 in the conventional strong LoS mmWave system without RISs. Although the RPG offers a high effective rank, Fig. 6 demonstrates that its truncated condition number is large as well. Consequently, RPG will not produce a satisfactory SE, as will be demonstrated in Fig. 9. Moreover, the effective rank cannot be customized according to the number of data streams once RISs are randomly designed. When path gains are designed to be homogeneous, the CDF of the effective rank for HPG is matched well with that of s in the low s regime. In other words, the proposed channel customization scheme can shape the composite channel to have an effective rank that is almost identical to the number of data streams. When s increases to 7 and 8, additional RISs are involved to provide extra sub-channel modes. In this case, the orthogonality of each sub-channel mode will be gradually impaired, thus resulting in a slightly inferior effective rank to the corresponding s . Considering that the effective rank is maximized by equal singular values, the CDF of the effective rank for MPG is more distorted when the path gains are optimized to be maximal but not homogeneous.

Fig. 6 shows the CDF of the truncated condition number, T_s , for the customized composite channel when s increases from 3 to 8. When the reflection phases of RISs are randomly designed, T_s in most channel realizations is large. For example, the presented CDF for RPG demonstrates that more than 70% of channel realizations have $T_s > 16$ even when s is reduced to 3. Therefore, we can conclude that the channel for RPG is

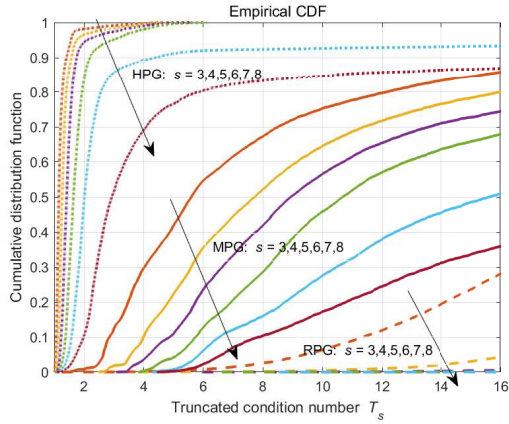


Fig. 6. CDF of T_s for the composite channel that has been customized according to s .

poorly conditioned for the purpose of communication. When the composite channel is customized according to s and the path gain of RIS k , $k \in \mathcal{K}_\perp$, is configured as maximum, the CDF for MPG improves dramatically. Specifically, the probability for $T_3 < 16$ is promoted to over 85%. Although CDFs for MPG drop when s increases, they are still superior to that for RPG. When the path gains of the active RISs in \mathcal{K}_\perp are designed to be homogeneous, T_s can be reduced well, as can be seen from CDFs for HPG. When s equals the maximal rank, that is 8, the probability for $T_8 > 16$ is cut down to less than 15%. Notably, when $s \leq 6$, the probability for $T_s \leq 8$ is nearly 100%, which means that the composite channel is conditioned well.

Fig. 7 illustrates the distribution of the truncated condition number in the circular coverage when the reflection phases of RISs are randomly designed. The left and right sub-figures are presented with $s = 2$ and $s = 4$, respectively. The upper sub-figures show the full range of T_s , while the bottom sub-figures only present $T_s \leq 8$, which is defined as well-conditioned in the following. Fig. 7(a) and 7(b) demonstrates that T_s distributes uniformly in the coverage and the distribution is similar for different s . Given that most T_2 and T_4 range from 10 to 100, we know that only one large singular value exists and the rest of singular values are small and in the same order of magnitude. To display the coverage with the well-conditioned channel, Fig. 7(c) and 7(d) remove $T_s > 8$. When $s = 2$, a few points remain with the well-conditioned channel. However, these points rapidly disappear when s increases to 4, thus indicating that the well-conditioned channel with a high rank cannot be customized with the randomly designed RISs.

In Fig. 8, the channel rank is customized according to the required number of data streams, and the path gains are tuned to be homogeneous. Compared with Fig. 7, the range of T_s decreases dramatically over the entire coverage. In addition, the well-conditioned channel can be established in every corner of the coverage. Thus, the proposed channel customization scheme is validated. More importantly, this desired channel is robust against the increasing s . For example, the maximal T_s only increases from 4.5 to 5, as can be seen in Fig. 8(a) and 8(b).

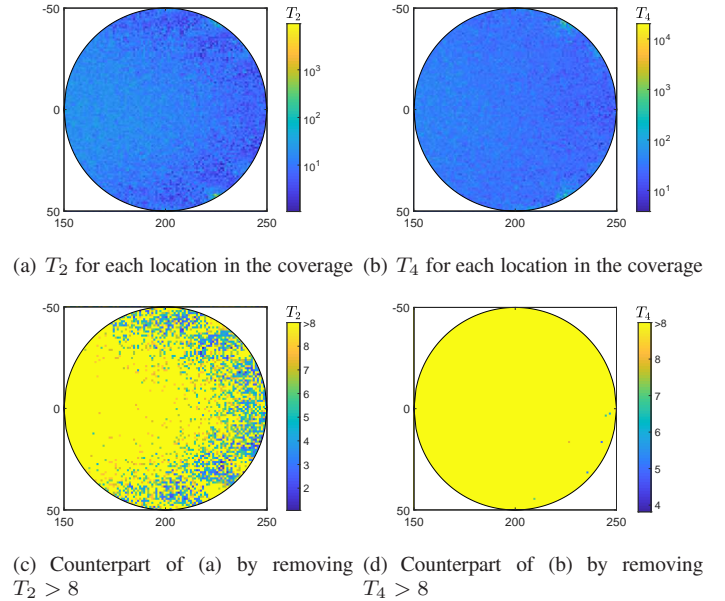


Fig. 7. Distribution of T_s in the coverage for RPG.

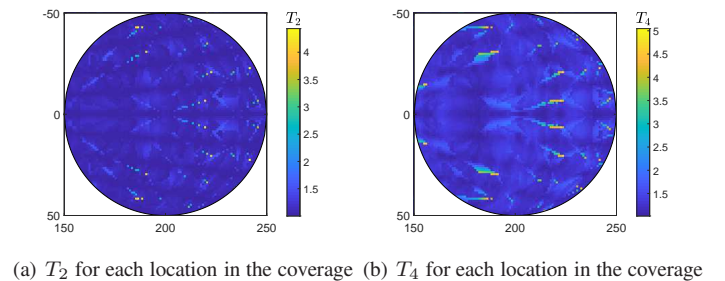
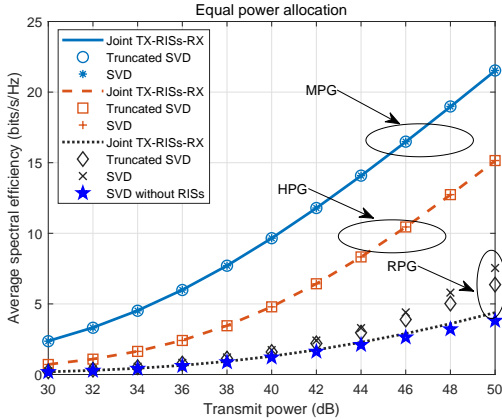


Fig. 8. Distribution of T_s in the coverage for HPG.

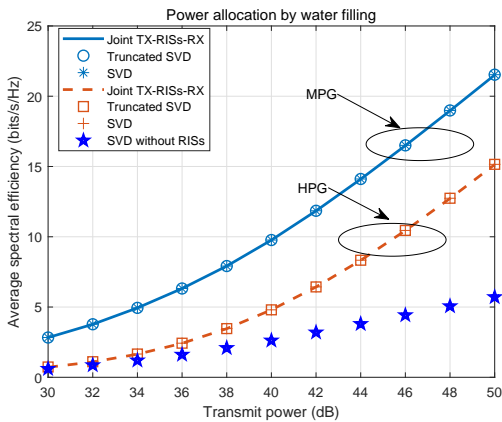
B. Joint Tx-RISs-Rx Design

In this subsection, the proposed joint Tx-RISs-Rx design is investigated in terms of the SE averaged over the entire coverage area. The SVD- and truncated SVD-based beamforming at the Tx and Rx are considered comparisons. In the following figures, the legends **SVD** and **Truncated SVD** indicate that beamforming matrices at the Tx and Rx are designed as $\{\mathbf{F}_{\text{RF}}\mathbf{F}_{\text{BB}} = \mathbf{V}\mathbf{P}^{1/2}, \mathbf{W}_{\text{RF}}\mathbf{W}_{\text{BB}} = \mathbf{U}\}$ and (39), respectively. The difference is that the **SVD** does not consider the limit on the number of RF chains as the **Truncated SVD** does. Notably, the matrix decomposition for digital and analog beamforming is not considered for the **SVD** and **Truncated SVD**.

Fig. 9 demonstrates the average SE versus transmit power for different RIS designs when $s = 4$. Evidently, the introduction of RISs brings substantial gains, especially in MPG cases, over the conventional systems without RISs. In Fig. 9(a), when the reflection phases of RISs are randomly designed, the SVD-based scheme achieves the best performance, whereas our proposal is the worst. The composite channel is not rectified well for multi-stream transmission. Hence, even when hybrid beamformings at the Tx and Rx focus on the orthogonal RISs, the transmitted



(a)



(b)

Fig. 9. Average SE versus transmit power for different RISs design with (a) equal power allocation and (b) water-filling power allocation.

energy is still dispersed. Although the effective rank for RPG is impressive in Fig. 5, the average SE of RPG is the worst compared with that of MPG and HPG, thus validating our conclusion that the high effective rank offered by the randomly designed RISs cannot produce a satisfactory communication performance. When the composite channel is carefully customized according to the data stream requirement, the performances of the joint Tx-RISs-Rx can be remarkably improved, regardless of power allocation schemes. Moreover, our proposal achieves almost identical SE to the SVD-based scheme without further matrix decomposition for digital and analog beamforming. Although HPG can establish a well-conditioned channel as shown in Fig. 8, the SE is inferior to that of MPG. This difference is a consequence of the reduction of the array gains of active RISs when their corresponding path gains are forced to be homogeneous.

Fig. 10 compares the average SE of equal power allocation and water-filling power allocation with increasing s when MPG is considered. Evidently, the increment of s can promote the average SE because additional sub-channel modes are excavated for multi-stream transmission. Considering that the water level must not decrease to ensure the equal power allocation is asymptotically

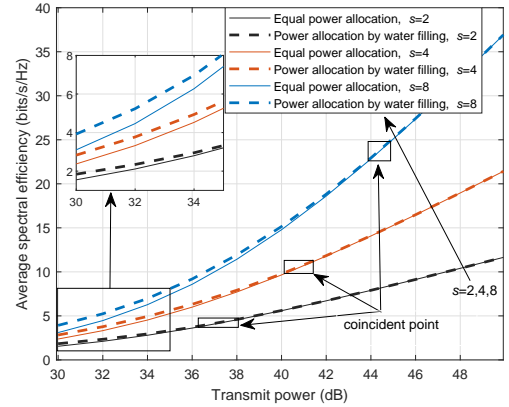


Fig. 10. Comparisons of the average SE for equal power allocation and water-filling power allocation with increasing s when MPG is considered.

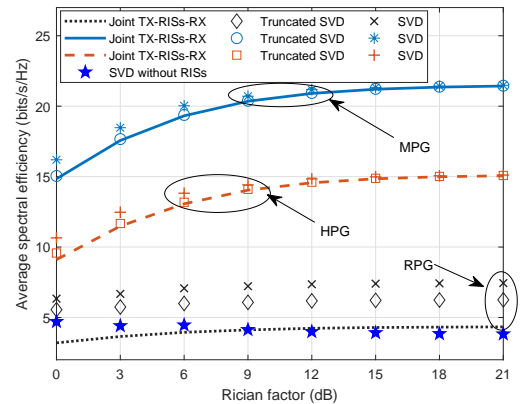


Fig. 11. Average SE versus Rician factor for different RISs design.

optimal, the transmit power should increase to compensate for the water decline when another sub-channel mode that has a lower bottom than the direct link is introduced. As a result, the coincident point for equal power allocation and water-filling power allocation shifts to higher transmit power.

C. Effect of NLoS Paths

In this subsection, the effect of NLoS paths on the proposed joint Tx-RISs-Rx design is investigated by relaxing the infinite Rician factor assumption. Considering the sparse nature of mmWave channels, the number of NLoS paths is set to 3 for $\mathbf{H}_{T,k}$, $\mathbf{H}_{R,k}$, and \mathbf{H}_D . We can safely assume that the power of the LoS component is larger than that of NLoS components in the strong LoS mmWave systems. Hence, in Fig. 11 we start the Rician factor from 0 dB. When the composite channel is customized well by MPG or HPG, the average SE of our proposal is slightly lower than the optimal SVD-based scheme at first but the performance gap is rapidly narrowed with the increasing Rician factor. Given that the limit on RF chains is not considered in the SVD-based scheme, our proposal still has a satisfactory

performance because it matches well with the truncated SVD-based scheme. Notably, when RISs are randomly designed in the scenario where the powers of the LoS component and NLoS components are comparative, our proposal is invalid because the directional energy transmitted to RISs is scattered. Nevertheless, the SVD- and truncated SVD-based scheme in the RISs-assisted system retain considerable performance gains than the counterpart without RISs, regardless of how RISs are designed.

VI. CONCLUSION

In this study, we investigated the channel customization and joint Tx-RISs-Rx design in the hybrid mmWave communication system assisted by distributed RISs. Sparse propagation paths in the conventional mmWave system result in a rank-deficient channel that is unpopular for multi-stream transmission. To overcome this intrinsic limitation, RISs were introduced to the customization of a favorable composite channel by reconfiguring its characteristics. Different from existing works, we provided a closed-form expression that bridges the singular value of the composite channel and the reflection phase of RISs to instruct the customization process. Furthermore, a low-complexity joint Tx-RISs-Rx design was proposed, which guaranteed the required effective channel rank for multi-stream transmission by configuring the reflection phases of RISs and performing the SVD-based hybrid beamforming without matrix decomposition. Numerical results demonstrated that the effective channel rank can be accurately and flexibly customized according to the number of data streams. In terms of the average spectral efficiency, the joint Tx-RISs-Rx design was shown to be able to obtain significant gains over the conventional system without RISs.

REFERENCES

- [1] C. E. Shannon, "A mathematical theory of communication," *Bell Syst. Tech. J.* vol. 27, pp. 379-423, July 1948.
- [2] E. Telatar, "Capacity of multi-antenna Gaussian channels," *Eur. Trans. Telecommun.*, vol. 10, no. 6, pp. 585-595, Nov. 1999.
- [3] Y. S. Cho, J. Kim, W. Y. Yang, and C. G. Kang, *MIMO-OFDM Wireless Communications with MATLAB*. Singapore: John Wiley & Sons (Asia) Pte Ltd, 2010.
- [4] D. Soldani, "5G beyond radio access: a flatter sliced network," *Mondo Digitale*, AICA, Mar. 2018.
- [5] W. Chen, Y. Han, S. Jin, and H. Sun, "Efficient multiband channel reconstruction and tracking for hybrid mmWave MIMO systems," *IEEE Trans. Commun.*, early access.
- [6] R. Baldemair *et al.*, "Ultra-dense networks in millimeter-wave frequencies," *IEEE Commun. Mag.*, vol. 53, no. 1, pp. 202-208, Jan. 2015.
- [7] M. R. Akdeniz *et al.*, "Millimeter wave channel modeling and cellular capacity evaluation," *IEEE J. Sel. Areas Commun.*, vol. 32, no. 6, pp. 1164-1179, Jun. 2014.
- [8] W. Chen, S. He, Q. Xu, and L. Yang, "Multi-beam receive scheme for millimetre wave wireless communication system," *IET Commun.*, vol. 13, no. 2, pp. 216-222, Jan. 2019.
- [9] Z. Xiao, X. Xia, D. Jin, and N. Ge, "Iterative eigenvalue decomposition and multipath-grouping Tx/Rx joint beamformings for millimeter-wave communications," *IEEE Trans. Wireless Commun.*, vol. 14, no. 3, pp. 1595-1607, Mar. 2015.
- [10] Y. Han *et al.*, "Large intelligent surface-assisted wireless communication exploiting statistical CSI," *IEEE Trans. Vehicular Tech.*, vol. 68, no. 8, pp. 8238-8242, Aug. 2019.
- [11] Q. Wu and R. Zhang, "Intelligent reflecting surface enhanced wireless network via joint active and passive beamforming," *IEEE Tans. Wireless Commun.*, vol. 18, no. 11, pp. 5394-5409, Nov. 2019.
- [12] M. Di Renzo *et al.*, "Smart radio environments empowered by reconfigurable AI meta-surfaces: An idea whose time has come," *EURASIP J. Wireless Commun. Networking*, 2019. vol. 2019, no. 129, May 2019.
- [13] M. Nemat, J. Park, and J. Choi, "RIS-assisted coverage enhancement on millimeter-wave cellular networks," *IEEE Access*, vol. 8, pp. 188171-188185, 2020.
- [14] W. Chen, X. Yang, S. Jin, and P. Xu, "Sparse array of sub-surface aided block-free multi-user mmWave communication systems," *Digit. Commun. Netw.*, vol. 6, no. 3, pp. 292-303, Aug. 2020.
- [15] W. Tang *et al.*, "Wireless communications with reconfigurable intelligent surface: Path loss modeling and experimental measurement," *IEEE Trans. Wireless Commun.*, vol. 20, no. 1, pp. 421-439, Jan. 2021.
- [16] W. Tang *et al.*, "Path loss modeling and measurements for reconfigurable intelligent surfaces in the millimeter-wave frequency band," [Online]. Available: <https://arxiv.org/abs/2101.08607>.
- [17] F. Shu *et al.*, "Enhanced secrecy rate maximization for directional modulation networks via IRS," [Online]. Available: <https://arxiv.org/abs/2008.05067v1>.
- [18] X. Mu, Y. Liu, L. Guo, J. Lin, and N. Al-Dhahir, "Exploiting intelligent reflecting surfaces in NOMA networks: Joint beamforming optimization," *IEEE Trans. Wireless Commun.*, vol. 19, no. 10, pp. 6884-6898, Oct. 2020.
- [19] H. Guo, Y.-C. Liang, J. Chen, and E.G. Larsson, "Weighted sum-rate maximization for intelligent reflecting surface enhanced wireless networks," in *Proc. 2019 IEEE Global Communications Conference*, Waikoloa, HI, USA, 2019, pp. 1-6.
- [20] C. Huang *et al.*, "Reconfigurable intelligent surfaces for energy efficiency in wireless communication," *IEEE Trans. Wireless Commun.*, vol. 18, no. 8, pp. 4157-4170, Aug. 2019.
- [21] Q.-U.-A. Nadeem *et al.*, "Asymptotic max-min SINR analysis of reconfigurable intelligent surface assisted MISO systems," *IEEE Trans. Wireless Commun.*, vol. 19, no. 12, pp. 7748-7764, Dec. 2020.
- [22] M.-M. Zhao, A. Liu, Y. Wan, and R. Zhang, "Two-timescale beamforming optimization for intelligent reflecting surface aided multiuser communication with QoS constraints," *IEEE Trans. Wireless Commun.*, early access.
- [23] S. Huang, S. Wang, R. Wang, M. Wen, and K. Huang, "Reconfigurable intelligent surface assisted mobile edge computing with heterogeneous learning tasks," *IEEE Trans. Cogn. Commun. Netw.*, vol. 7, no. 2, pp. 360-382, Feb. 2021.
- [24] P. Wang, J. Fang, L. Dai, and H. Li, "Joint transceiver and large intelligent surface design for massive MIMO mmWave systems," *IEEE Trans. Wireless Commun.*, vol. 20, no. 2, pp. 1052-1064, Feb. 2021.
- [25] X. Yang, C.-K. Wen, and S. Jin, "MIMO detection for reconfigurable intelligent surface-assisted millimeter wave systems," *IEEE J. Sel. Areas Commun.*, vol. 38, no. 8, pp. 1777-1792, Aug. 2020.
- [26] A. Abrardo, D. Dardari, and M. D. Renzo, "Intelligent reflecting surfaces: Sum-rate optimization based on statistical CSI," [Online]. Available: <https://arxiv.org/abs/2012.10679v1>.
- [27] B. Zheng, C. You, and R. Zhang, "Double-IRS assisted multi-user MIMO: Cooperative passive beamforming design," *IEEE Trans. Wireless Commun.*, vol. 20, no. 7, pp. 4513-4525, Feb. 2021.
- [28] M. A. ElMossallamy, H. Zhang, R. Sultan, K. G. Seddik, L. Song, G. Y. Li, and Z. Han, "On spatial multiplexing using reconfigurable intelligent surface," *IEEE Wireless Commun. Lett.* vol. 10, no. 2, pp. 226-230, Feb. 2021.
- [29] P. d. Hougne, M. Fink, and G. Lerosey, "Optimally diverse communication channels in disordered environments with tuned randomness," *Nat. Electron.*, vol. 2, pp. 36-41, Jan. 2019.
- [30] M. R. Akdeniz *et al.*, "Millimeter wave channel modeling and cellular capacity evaluation," *IEEE J. Sel. Areas in Commun.*, vol. 32, no. 6, pp. 1164-1179, June 2014.
- [31] W. Chen, C.-K. Wen, X. Li, and S. Jin, "Adaptive bit partitioning for reconfigurable intelligent surface assisted FDD systems with limited feedback," [Online]. Available: <https://arxiv.org/abs/2011.14748>.
- [32] M. Jung, W. Saad, Y. Jang, G. Kong and S. Choi, "Performance analysis of large intelligent surfaces (LISs): Asymptotic data rate and channel hardening effects," *IEEE Trans. Wireless Commun.*, vol. 19, no. 3, pp. 2052-2065, Mar. 2020.
- [33] O. Ozdogan, E. Bjornson, and E. G. Larsson, "Intelligent reflecting surfaces: Physics, propagation, and pathloss modeling," *IEEE Wireless Commun. Lett.*, vol. 9, no. 5, pp. 581-585, May 2020.
- [34] K. Keykhosravi and H. Wymeersch, "Multi-RIS discrete-phase encoding for interpath-interference-free channel estimation," [Online]. Available: <https://arxiv.org/abs/2016.07065v1>.
- [35] W. Chen, L. Bai, W. Tang, S. Jin, W. X. Jiang, and T. J. Cui, "Angle-dependent phase shifter model for reconfigurable intelligent surfaces: Does the angle-reciprocity hold?" *IEEE Commun. Lett.*, vol. 24, no. 9, pp. 2060-2064, Sept. 2020.
- [36] Z. Muhi-Eldeen, L. P. Ivrisimtzis, and M. Al-Nuaimi, "Modelling and measurements of millimetre wavelength propagation in urban environments," *IET Microw. Antennas Propag.*, vol. 4, no. 9, pp. 1300C1309, Sep. 2010.
- [37] O. Roy and M. Vetterli, "The effective rank: A measure of effective dimensionality," in *2007 15th European Signal Processing Conf.*, 2007, pp. 606-610.
- [38] I. Gradshteyn and I. Ryzhik, *Table of Integrals, Series, and Products*. Academic Press, 1980.

- [39] S. park, A. Alkhateeb, and R. W. Heath, "Dynamic subarray for hybrid precoding in wideband mmWave MIMO systems," *IEEE Trans. Wireless Commun.*, vol. 16, no. 5, pp. 2907-2920, May 2017.
- [40] H. Wolkowicz and G. P. H. Styan, "Bounds for eigenvalues using traces," *Linear Algebra Appl.*, no. 29, pp. 471-506, Feb. 1980.